CLEAN
Soil Air Water

Renewables

Sustainability

Environmental Monitoring

Sofía Schlichter
Alejandra S. Diez
María C. Zenobi
Mariana Dennehy
Mariana Alvarez

INQUISUR, Departamento de Química, Universidad Nacional del Sur, Bahía Blanca, Argentina

Research Article

Multi-Metal-Substituted-Goethite as an Effective Catalyst for Azo Dye Wastewater Oxidation

Different samples of goethite modified with cobalt, manganese, or aluminum were synthesized and characterized by means of X-ray diffraction, chemical analysis, scanning electron microscopy, zeta potential measurements, and N_2 adsorption–desorption isotherm analysis. The goethite oxides were tested as efficient catalysts for the degradation of methyl orange (MO, sodium 4-[(4-dimethylamino)phenylazo] benzenesulfonate), a sulfonated azo dye indicator, employing potassium persulfate (PS) in water, at pH 3. The Mn, Co, and Al substitution in goethite gave rise to active sites for PS activation. The most effective catalyst reached 93% of degradation at 120 min of reaction. The increase of temperature led to an expected conversion enhancement, and kinetic parameters were calculated for one of the evaluated catalysts. MO degradation curves best fitted to pseudo-second order kinetics. The extent of mineralization, measured as total removed organic carbon (TOC), was also monitored. A significant degree of mineralization was achieved and confirmed by TOC analysis. A mechanism for MO oxidation with $SO_4^{\bullet-}$ radicals was discarded and a pathway involving peroxymonosulfate species was proposed. The results indicate that the goethite-substituted oxides are effective catalysts for the studied azo dye degradation in aqueous solution.

Additional supporting information may be found in the online version of this article at the publisher's web-site.

1 Introduction

Azo dyes with at least one azo group ($-N{=}N-$) represent the largest group of synthetic dyes employed in many industries [1]. Particularly, the textile industries use azo dyes with one or more azo bonds with simple or multiple aromatic groups [2]. About 10–20% of dyes in the textile sector are lost in residual liquors through incomplete exhaustion and washing operations. Most of these dyes are non-biodegradable, toxic, and potentially carcinogenic in nature. Methyl orange (MO, 4-[4-(dimethylamino)phenylazo]benzenesulfonic acid) is a water soluble sulfonated azo dye (Fig. 1) which is employed globally in coloring textiles.

Oxidation processes are progressively followed to eliminate organic contaminants in a variety of wastewaters from different industrial plants. The employment of heterogeneous catalysts for oxidation is presented as an effective procedure for removing stable organic compounds including dye molecules [3–5]. Persulfate (PS) anions, $S_2O_8^{2-}$, are one of the strongest oxidants known in aqueous solutions, showing higher potential ($E^0 = 2.05$ V) than H_2O_2 ($E^0 = 1.76$ V). This offers some advantages over other oxidants since PS is solid at ambient temperature, is highly stable for storage and transportation, and has high aqueous solubility and is of relatively low cost. Even more, SO_4^{2-}, which is the product of the reaction, is practically inert and is not considered to be a pollutant. However, direct reaction of PS with most reductants is slow and the employment of a heterogeneous catalyst is fundamental for developing an oxidation process using PS as oxidant. Low cost materials employed as catalysts for the removal of pollutants in effluents are becoming increasingly interesting for environmental protection [6–9]. In this context, catalysts based on iron oxides have arisen as an attractive alternative [10–14]. Iron oxides are abundant low cost materials, they are stable, reusable, and environmentally friendly. In particular, the ability and potential of iron oxides to catalyze the oxidation of organic compounds through the Fenton-like reaction have been well documented [15–23]. Thermodynamically, goethite (α-FeOOH) is a very stable iron oxide. Regarding heterogeneous Fenton processes, goethite can be considered as an efficient catalyst, attributable to its properties, such as stability at pH >2, scarce iron leaching, elevated surface OH groups concentration, and abundance [24–27]. The goethite structure consists of a close-packed array of O^{2-} and OH^- with Fe^{3+}, similar

Correspondence: Dr. Mariana Alvarez, INQUISUR, Departamento de Química, Universidad Nacional del Sur, Avda. Alem 1253, B8000CPB, Bahía Blanca, Argentina
E-mail: alvarezm@criba.edu.ar

Abbreviations: BET, Brunauer–Emmett–Teller; FTIR, Fourier transform infrared spectroscopy; IEP, isoelectric point; MO, methyl orange; PS, persulfate; PZC, point of zero charge; SEM, scanning electron microscopy; SSA, specific surface area; TOC, total organic carbon; XRD, X-Ray diffraction.
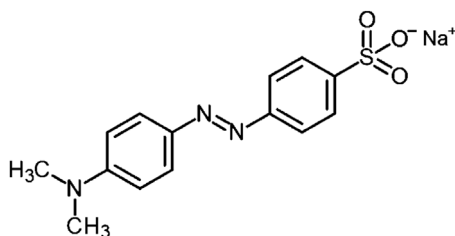
Figure 1. Structure of methyl orange (MO).

to the diaspore structure. The sixfold coordinated Fe has been demonstrated to be usually replaced by Al, Co, Mn, Cr, Ni, etc. [28]. The metal substitution for Fe significantly affects the physicochemical properties of goethite. As it is well known, single metal-for-Fe substitution has been the subject matter of numerous studies. However, there are not many reports regarding multiple metal substitutions in goethite [29–33]. Manceau et al. [30] reported the simultaneous substitution of Cr, Mn, Co, Ni, Cu, and Zn in natural goethite. On the other hand, Cornell [29] found a higher inclusion of 8 mol% for Ni, Co, and Mn, and Kaur et al. [32] reported a maximum value of 10.5 mol% for Cr, Zn, Cd, and Pb, into the framework of a synthetic oxyhydroxide. Those limits represent both synergistic and antagonistic incorporation effects. Concerning aluminum and manganese inclusion in goethite, a previous article has shown the dominance of Mn over Al in the simultaneous incorporation of both ions in the goethite structure [31].

Natural goethites as well as synthetic samples have been used for the remediation of different organic pollutants. Recently, a research was published regarding the use of pure goethite as a Fenton catalyst for the MO degradation [16]. However, to our knowledge, scarce reports exist in the literature regarding substituted goethites applied as catalysts for the azo dye degradation using PS. For this reason, in the present work, a study was carried out regarding the activity of a series of substituted goethites as catalysts for the oxidative MO degradation. Thus, Mn-, Co-, and Al-goethites were synthesized, since these metal cations coexist with goethite in natural systems, and the determination of their catalytic properties is of great interest. Besides, transition metal cations (Mn^{2+}, Co^{2+}, etc.) are known as an alternative for PS activation. Samples were tested for the MO degradation employing PS anion as the oxidant in water, and their characterization was carried out by X-ray diffraction (XRD), Fourier transform infrared spectroscopy (FTIR), scanning electron microscopy (SEM), electrophoretic mobility, and nitrogen sorptometry for measuring specific surface area from Brunauer–Emmett–Teller (BET) method.

An attempt to postulate a possible mechanism for the MO degradation over the goethite surface was carried out based on both the characterization results and the catalytic tests.

2 Materials and methods

All chemicals were of analytical reagent grade and were used as purchased.

2.1 Goethite preparation

Two series of Me-goethites, (Mn–Co)-goethites and (Co–Al)-goethites, were prepared as described elsewhere [34]. The target metal content χ_{Me} was kept constant at 12%:

$$X_{Me} = mol\ Me \times 100/(mol\ Me + mol\ Fe) \qquad (1)$$

in order to avoid the formation of other phases except goethite.

2.1.1 Co−Mn-goethites

Single Mn-, Co-, and mixed Mn−Co-goethites were prepared from ferrihydrite by adding 2 M NaOH to a Fe(III) + Mn(II) + Co(II) nitrate solution (Me/OH⁻ = 0.076). In all cases, the initial total metal concentration achieved was 0.53 M. The precipitates were washed with water, centrifuged and mixed with 0.3 M NaOH and left for 15 days at 60°C in closed Teflon flasks.

2.1.2 Co−Al-goethites

Al-goethite was prepared by mixing 25 mL of solution A (1 M Fe(NO₃)₃), 29.6 mL of solution B (0.5 M Al(NO₃)₃, 62.5 mL + 5 M KOH, 37.5 mL, ratio [OH⁻]/[Al] = 6), and 45 mL of 5 M KOH. Co−Al-goethites with different Co/Al molar ratios (9:3, 6:6, and 3:9) were obtained by mixing solutions A and B with appropriate volumes of 0.5 M Co(NO₃)₂, followed by the addition of 5 M KOH. According to the same procedure, an additional tri-substituted sample was synthesized with Co/Al/Mn, 4:4:4.

In all cases, Teflon bottles were used, and bidistilled water was added to reach a final KOH concentration of 0.3 M. Once again, the suspensions were left for 15 days at 60°C.

In both series of samples, bottles were daily opened, recapped, and shaken by hand end-over-end for 5 s. Thereafter, the materials were washed with bidistilled water until the conductivity of the filtered solution was similar to that of the bidistilled water. The remaining solids were dried at 40°C and gently crushed. The mixed samples were synthesized with different Co/Mn or Co/Al nominal molar ratios (12:0, 9:3, 6:6, 3:9, and 12:0%), and were named as $Co_xMn_yAl_z$, where x, y, and z correspond to the Co, Mn, and Al molar percentage (as measured by atomic absorption spectroscopy, AAS), respectively.

2.2 Characterization of solids

The metal content in all samples was calculated by atomic absorption spectrometry (GBC Model B-932). Here, 30 mg of each solid were dissolved in 6 M HCl at 80°C. The IR spectra of the substances as KBr pellets were recorded in a 4000−400 cm⁻¹ range (Nicolet Nexus FTIR spectrometer). The specific surface area (SSA) of the samples was measured (Micrometrics AccuSorb 2100) using N_2 as the absorbate (BET method). Diffraction patterns were recorded in a diffractometer (Siemens D5000) using Cu Kα radiation.

Generator settings were 40 kV, 35 mA. Divergence, scattered and receiving slits were 1°, 1°, and 0.2 mm, respectively. A curved graphite monochromator was used. Data were collected in a 2θ range: 18.5−130.5°, with scanning steps of 0.025° and a counting time of 15 s per point. Particle morphology was characterized using scanning electron microscopy (SEM) by examining a drop of suspension dried on a metallic support (Zeiss Supra 40, field emission, gun-scanning electron microscope). The isoelectric point (IEP) of the samples was obtained using a Malvern Zetasizer. The zeta potential of the oxides was measured in a pH range of 3.5–8.5, using a solution/solid ratio equal to 20 L g⁻¹ (10⁻² M NaNO₃). The pH value was adjusted by adding 0.1 M KOH or HNO₃.

2.3 MO degradation

The degradation reactions were performed in a glass reactor at room temperature (30°C), containing 150 mL of simulated wastewater, which was obtained by adding 10 mg L^{-1} of MO into a aqueous solution, pH 3. The pH was adjusted with H$_2$SO$_4$. In a typical procedure, the reaction was initiated by adding K$_2$S$_2$O$_8$ (200 mg L^{-1}) and 200 mg of the catalyst to the prepared reaction solution. These conditions were chosen according to the optimal conditions for MO degradation given in the literature [35]. The reaction was carried out under mechanical stirring. Time dependence of the MO degradation was measured. At designated sampling intervals (ca. 5 min), 3 mL of the solution were removed from the reaction vessel. Immediately, the aliquot was filtered with a syringe through a Nuclepore membrane (pore size 0.22 μm) and analyzed by UV-vis (Cecil 2021 spectrophotometer). The MO concentration in the reaction mixture at different reaction times was determined by measuring the absorption intensity at $\lambda_{max} = 506$ nm. Prior to this measurement, a calibration curve was obtained using MO solutions with known concentrations. During the experiments, the color of the solution changed from orange to almost colorless. All degradation experiments were carried out in duplicate. The MO mineralization was established on the basis of total organic carbon (TOC) content, performed by using a Shimadzu TOC-L CPH/CPN analyzer, after the sample was quenched by 3 M sodium nitrite. The percentage of MO conversion, X%, was taken as measurement of catalyst degradation efficiency [36] toward MO according to the following definition:

$$X\% = \left(1 - \frac{C_t}{C_0}\right) \times 100 \qquad (2)$$

where C_0 (mg L^{-1}) is the initial MO concentration, and C_t (mg L^{-1}) is the MO concentration at reaction time, t (min).

To monitor metal leaching from the catalyst, samples were filtered with 0.22 μm filters at the end of the reaction, and analyzed with atomic absorption spectrophotometry (GBC Model B-932).

In order to determine the radical species formed by the metal-oxidant couple, two sets of quenching experiments were performed. The experimental procedures were repeated with the addition of 6.3 mL of *tert*-butyl alcohol and 3.9 mL of ethanol, in two separate experiences (alcohol/oxidant, 600:1). Each alcohol was added to the reactor before adding the catalyst. Reusability was tested in Co$_{2.4}$Al$_{3.1}$Mn$_{2.8}$ by

recovering the solid from the reaction mixture, washing it thoroughly with distilled water and drying it overnight before the next run, with a constant dye/catalyst/oxidant mass ratio (1:133:20).

3 Results and discussion

3.1 Characterization of samples

Metal concentrations and specific surface area (SSA) of the samples are summarized in Tab. 1. The SSA of the goethites has significantly changed after metal incorporation. It can be observed that Co incorporation leads to a marked increase, with a maximum value shown for the single-substitution of Co-for-Fe (109 ± 1 m^2 g^{-1}). On the other hand, addition of Mn originates a remarkable decrease in SSA, and samples with only Mn (Co$_0$Mn$_{10.1}$) presented the minimum SSA value (28 ± 1 m^2 g^{-1}). These oxides with di-substitution had increments in SSA with increasing Co content and decreasing Mn content. The same trend as for Mn was detected for Al incorporation. The Al-substituted goethite (Co$_0$Al$_{8.5}$) showed the lowest SSA (26 ± 1 m^2 g^{-1}). The tri-substituted oxy(hydr)oxide showed high SSA, related to the strong influence of Co incorporation (64 ± 1 m^2 g^{-1}) [34].

The pH of the medium has a strong effect on the particles charge. The pH at which the charge on the surface is zero is referred to as the point of zero charge (PZC) or the IEP, but these terms can only be used in the same way if there is no specific adsorption. The isoelectric point is the pH at which the net surface charge is zero, that is, the positive and negative charges arising from all sources are equal. It is measured by electrophoresis and corresponds to the pH at which there is no motion of the particles in an electric field [28, 37].

The partial substitution of Fe(III) by foreign cations could generate variations in the IEP value with regard to pure goethite. For both series of samples, the IEP values were quite similar compared to α-FeOOH (IEP = 7.3). However, two samples, Co$_0$Mn$_{10.1}$ and Co$_0$Al$_{8.5}$, clearly showed lower IEP values. The measured value for the first sample (5.8) is coherent with values reported for Mn oxides (<5) [38] and could indicate that Mn is mainly distributed in the external layers of the crystals. In the case of Co$_0$Al$_{8.5}$ sample, the IEP value was 5.2, and this could be due to the different acid/base characteristics of the Al−OH and Fe−OH superficial species [39].

SEM micrographs of selected samples of both series are presented in Fig. 2. The average length of goethite acicular crystals increased,

Table 1. Specific surface area and catalytic properties for MO oxidation at 30°C for pure and substituted goethite catalysts

Sample	Phases	SSA (m^2 g^{-1})	IEP	%X[a]	Rate[b] (μg m^2 min^{-1})
Co$_0$Mn$_0$Al$_0$	Goethite	36 ± 1	7.3	18	2.7
Co$_{7.9}$Mn$_0$	Goethite	109 ± 1	7.4	86	2.8
Co$_{6.9}$Mn$_{2.2}$	Goethite	58 ± 1	n.d.	79	4.1
Co$_{5.0}$Mn$_{5.0}$	Goethite	55 ± 1	7.8	49	3.8
Co$_{2.6}$Mn$_{7.6}$	Goethite	42 ± 1	n.d.	49	4.8
Co$_0$Mn$_{10.1}$	Goethite	28 ± 1	5.8	45	6.8
Co$_{6.1}$Al$_{2.1}$	Goethite, CoFe$_2$O$_4$	38 ± 1	n.d.	40	9.0
Co$_{4.2}$Al$_{3.5}$	Goethite, CoFe$_2$O$_4$	43 ± 1	7.3	24	3.5
Co$_{2.2}$Al$_{5.3}$	Goethite	36 ± 1	n.d.	43	12.0
Co$_0$Al$_{8.5}$	Goethite	26 ± 1	5.2	44	16.9
Co$_{2.4}$Al$_{3.1}$Mn$_{2.8}$	Goethite	64 ± 1	6.8	93	6.4

n.d., not determined.
[a] Percentage of conversion following 120 min of reaction time.
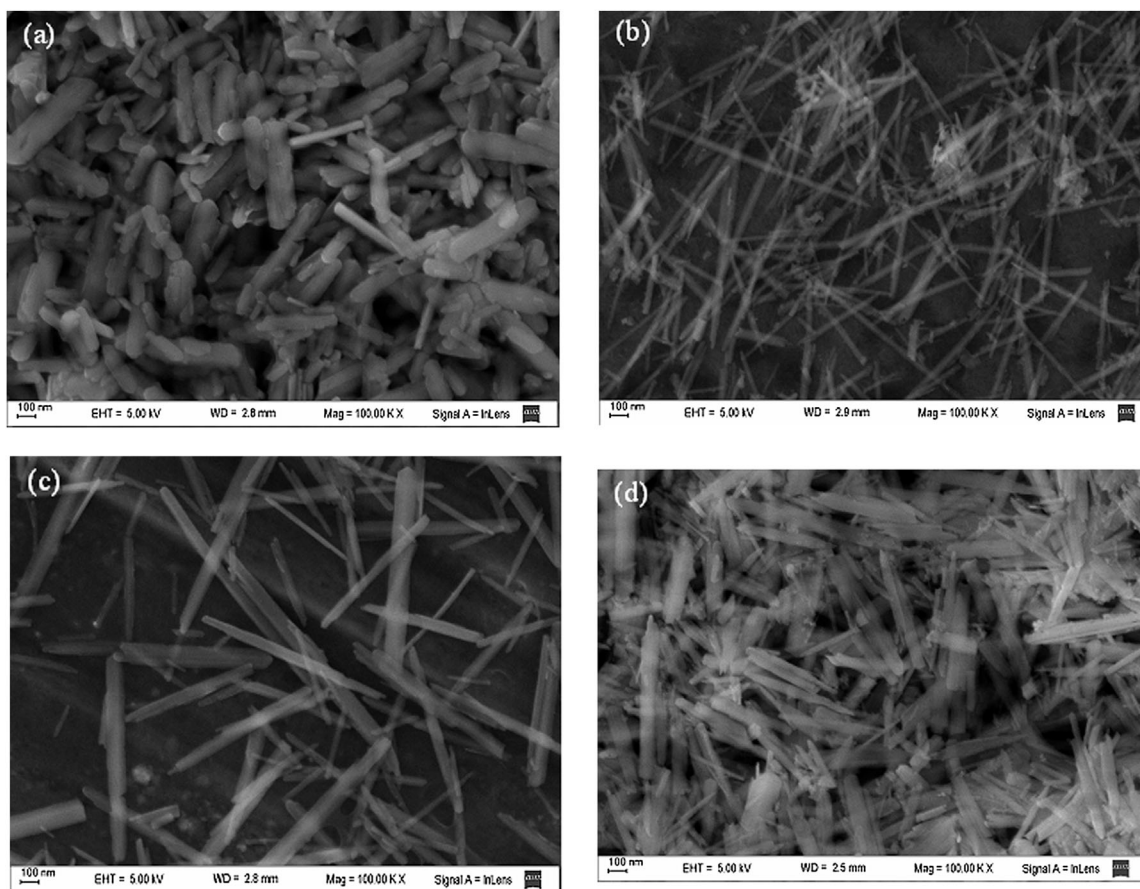[b] Measured at reaction times <10 min.

Figure 2. SEM images of samples (a) $Co_0Al_{8.5}$, (b) $Co_{7.9}Mn_0$, (c) $Co_0Mn_{10.1}$, and (d) $Co_{2.4}Al_{3.1}Mn_{2.8}$.

while the width diminished with the Co content ($Co_{7.9}Mn_0$), leading to thinner and longer crystals. The Mn containing goethite showed wider crystals than $Co_{7.9}Mn_0$, which is in line with the fact that the former catalyst develops lower SSA than the latter. The threefold substituted sample ($Co_{2.4}Al_{3.1}Mn_{2.8}$) presented a marked polydispersion that could indicate an inhomogeneous distribution of the cations within the oxide structure. These results are in agreement with earlier reports [31, 40].

The XRD patterns of all Co−Mn-goethite samples showed that goethite is the only phase present in these catalysts (Tab. 1). Slight reflections due to $CoFe_2O_4$ were observed in the pattern of $Co_{6.1}Al_{2.1}$ and $Co_{4.2}Al_{3.5}$. Increasing total metal substitution, the 101 peak shifted to greater d-spacing.

Shifts in the diffraction peaks of Me-substituted goethite indicated anisotropy in the lattice expansion/contraction due to metal substitution in the oxide structure. The XRD patterns of selected samples are presented in Fig. 3. (The XRD patterns for all samples are presented in Supporting Information Fig. S1).

3.2 MO degradation

3.2.1 Control experiments

In a typical procedure, the studied amount of PS ($200\,mg\,L^{-1}$) was added into a glass reactor containing MO solution, being stirred by magnetic force. At given intervals of reaction, aliquots were taken

out to be analyzed by UV-vis spectrophotometry. Only ca. 20% of the dye was decomposed after 70 min of reaction, showing that MO cannot be efficiently oxidized by PS only. This result is in agreement with previous reports [18, 41].

Furthermore, when only MO and a catalyst were added to the reactor, in absence of the oxidant PS, a maximum of 28% of dye decolorization was achieved after 120 min of reaction.

With the aim of verifying the influence of light over MO degradation, different experiments using selected catalysts ($Co_0Mn_{10.1}$ and $Co_{7.9}Mn_0$) were also performed in the dark. The reaction profiles were practically identical to those carried out in the presence of light, suggesting that the reaction was not photo-catalyzed.

3.2.2 Decolorization experiments

Table 1 shows the results of the oxidative MO degradation catalyzed by PS with goethite at 30°C, after 120 min of reaction. Pure goethite sample showed low conversion levels (<20%). On the other hand, all the substituted goethite samples showed higher conversion values than bare goethite, indicating that the substitution of Fe by Al, Co, and/or Mn in goethite develops active sites for MO degradation.

FTIR spectra of the catalysts before and after MO contact were recorded. As an example, the profiles corresponding to the $Co_{7.9}Mn_0$ test are presented in Fig. 4. FTIR spectrum of the MO dye is also shown.

Two intense bands due to the bulk hydroxyl stretch and the surface hydroxyl groups appear at ca. 3100 and $3400\,cm^{-1}$,
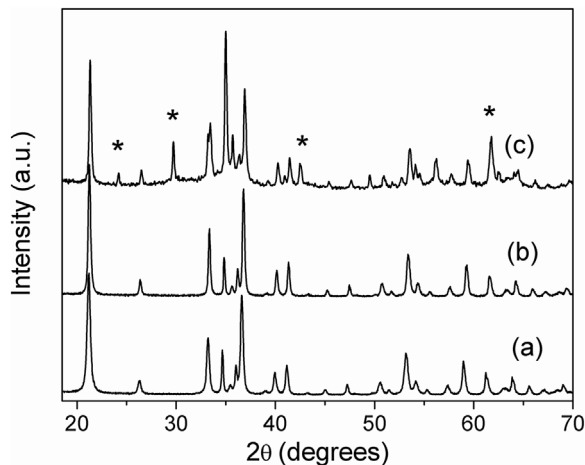
Figure 3. XRD patterns of (a) pure goethite, (b) $Co_{2.2}Al_{5.3}$, and (c) $Co_{6.1}Al_{2.1}$. *Indicate the presence of a spinel phase.

respectively. The bands at ca. 890 and 795 cm^{-1} correspond to OH bending vibrations.

As it is known, surface OH species of goethite are affected by pH [42]:

$$\equiv MeOH_2^+ \leftrightarrows \equiv MeOH + H^+. \tag{3}$$

From the IEP data, it is worth noting that the concentration of positively charged $\equiv MeOH_2^+$ species increased as the pH dropped. The surface charge of MO is generally negative because of the sulfonated group ($-SO_3^-$) [16]. Thus, the MO adsorption onto the iron oxide surface is favored at acidic pH, considering the electrostatic attraction [43]. However, the catalyst IR spectra before and after reaction are almost the same, showing that the reaction mainly occurs by a degradation rather than adsorption mechanism.

Due to the fact that, in general, the samples show different SSA values, a rate expressed as the mass of dye degraded per unit area of catalyst per unit time should be taken into account when comparing the activity of catalyst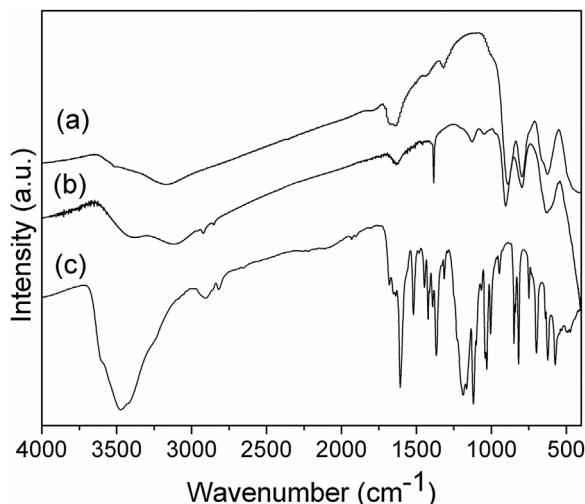s in order to describe the effect of each metal incorporation. The rates of the different catalysts are reported in Tab. 1.

In Fig. 5, the dependence of the specific rate on the Mn or Al mole concentration is shown. In general, for both series of oxides, the specific rate increases with the corresponding metal loading. It can be concluded that the active sites for MO oxidation are intimately associated with Mn or Al species in goethite. Furthermore, the increasing activity is more remarkable for Mn than for Al. The incorporation of Co would lead only to an increase in the SSA of the catalyst, as it was also shown for single-substituted oxides [40].

In the light of these results, it appeared opportune to synthesize and test a new three-heteroatom-goethite sample ($Co_{2.4}Al_{3.1}Mn_{2.8}$). This sample showed the highest conversion level, while its activity (evaluated from the specific rate) showed an intermediate value among all tested catalysts.

Figure 6 shows the influence of three different temperatures, 30, 40, and 50°C on the reaction, employing the tri-substituted $Co_{2.4}Al_{3.1}Mn_{2.8}$-goethite catalyst. The increment in the reaction temperature led to a conversion rise. At 10 min of reaction, 57, 67, and 71% of conversion were measured at 30, 40, and 50°C, respectively. As can be seen in Fig. 6, the three experiments reached a conversion of 93% at 120 min of reaction.

For the sake of comparison, the results corresponding to $Co_{7.9}Mn_0$ are also shown in Fig. 6 (at 30°C). It can be clearly observed that this catalyst developed lower conversion than the tri-substituted goethite catalyst ($Co_{2.4}Al_{3.1}Mn_{2.8}$) at short as well as at high reaction times.

In order to estimate the kinetic rates at different temperatures, the obtained data were treated with different kinetic models. The pseudo-second order kinetic equation proposed by Blanchard et al. [44] given in its linear form:

$$\frac{1}{C_t} = \frac{1}{C_e} + \left(\frac{1}{kC_e^2}\right)\frac{1}{t} \tag{4}$$

where C_t is the MO conversion degree (%) at time (t) and k is the pseudo-second order rate constant (min^{-1}). MO degradation curves best fitted to the pseudo-second order kinetics with high values of regression coefficients ($R^2 > 0.98$). Kinetic constants are presented in Tab. 2.
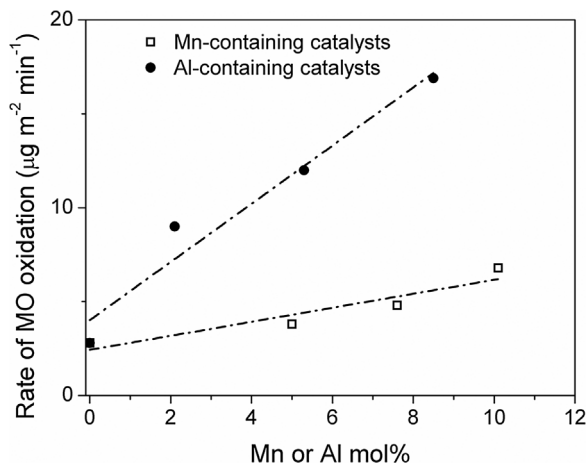

Figure 4. FTIR spectra of $Co_{7.9}Mn_0$ sample: (a) Before MO decolorization, (b) after MO decolorization, and (c) MO.

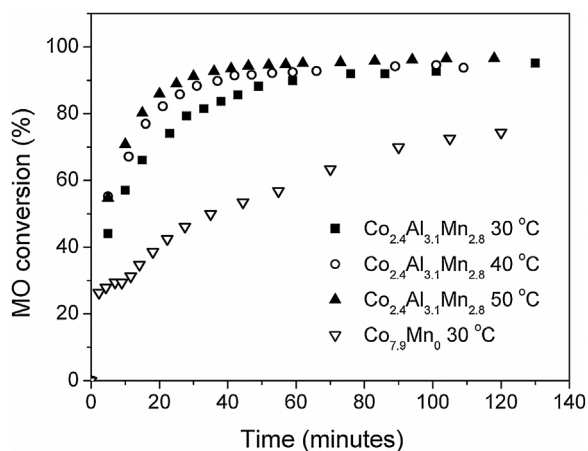**Figure 5.** Variation of the specific rate of MO degradation versus Mn or Al mol%.

Figure 6. Effect of the temperature on the degradation of MO using $Co_{2.4}Al_{3.1}Mn_{2.8}$ catalyst.

As can be seen from Tab. 2, the kinetic reaction rate increased with increasing temperature. The Arrhenius plot of rate constants versus T for $Co_{2.4}Al_{3.1}Mn_{2.8}$ presented a good linear correlation ($R^2 = 0.99$) and the activation energy was derived as $17 \pm 1\ kJ\ mol^{-1}$. This value is lower than those found for decolorization of the azo dye Orange G by using goethite/H_2O_2 as a heterogeneous Fenton-like reagent ($42\ kJ\ mol^{-1}$) [45], or nanoscale zerovalent iron particles used for MO degradation ($23\ kJ\ mol^{-1}$) [46].

It is known that the intermediate compounds that might be formed from MO degradation may be more toxic than the parent compound, as stated in [47]. The overall goal of the treatment processes should be the maximal mineralization to carbon dioxide, water and low concentrations of mineral acids (harmless end products), rather than just decolorization. For this reason, the changes in the profiles of the UV-vis MO spectra were investigated testing the $Co_{7.9}Mn_0$ catalyst. The UV-vis spectra of the sample $Co_{7.9}Mn_0$ recorded at 2, 6, and 24 h are shown in Fig. 7a together with the UV-vis spectrum of the MO initial solution (Fig. 7b).

Initially, an intense absorption band appeared at 506 nm, attributed to azonium ions, and two bands at 278 and 321 nm due to modification of the π system delocalization. At 2 h of reaction, these bands diminished (ca. 80%) indicating a partial degradation of the dye, while the highest degree of degradation (>90%) was achieved after 24 h of reaction.

In order to quantify the partial or total MO mineralization by PS, TOC removal experiments were conducted.

As can be seen from Fig. 8, TOC quickly diminished to 60% elimination within 2 h of reaction and an additional 20% reduction was observed after 24 h. These results indicated that the first stage of the reaction was fast, and the rate of reaction slowed down in a second period.

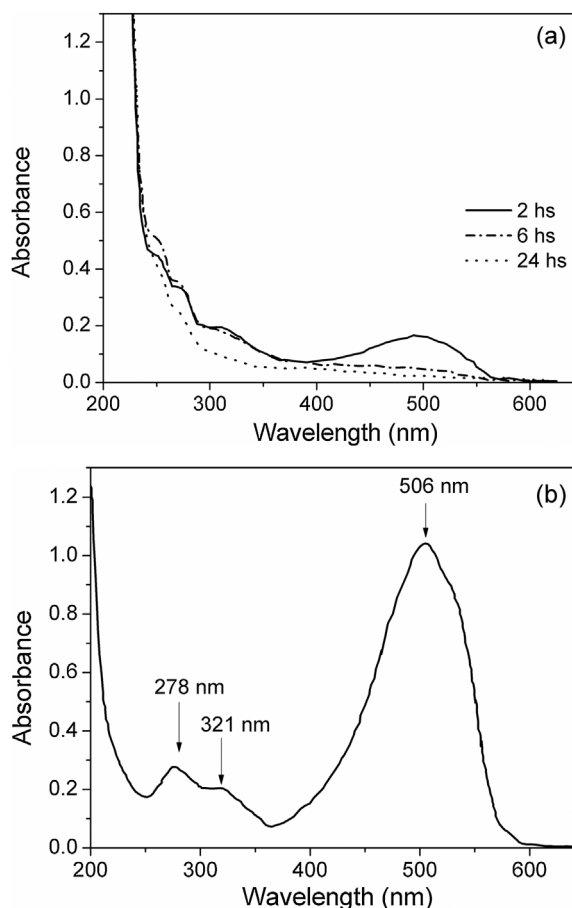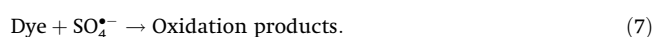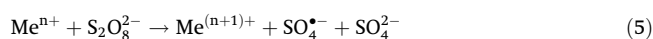**Figure 7.** UV-vis spectra of degradation of MO over $Co_{7.9}Mn_0$: (a) Temporal evolution of UV-vis spectra of MO solution, (b) initial UV-vis spectrum of MO solution.

In a recent article, Wang et al. [16] used a pure goethite/H_2O_2 system for MO degradation through a heterogeneous Fenton process and final levels of 55% TOC removal were attained. In this work, a higher level of mineralization was achieved using a substituted goethite sample.

In order to evaluate the reusability of the $Co_{2.4}Al_{3.1}Mn_{2.8}$ catalyst, the catalyst was recovered from the reaction mixture, washed thoroughly with distilled water, and dried overnight before the next run. The recycling test result showed a slight decrease of degradation (ca. 10% at 120 min) (Supporting Information Fig. S2).

The activation of PMS catalyzed by transition metals generates three main types of reactive radicals, namely sulfate, hydroxyl, and peroxy-sulfate radicals. A reaction mechanism, involving $SO_4^{\bullet-}$ radicals, has been suggested in the literature as follows [48]:

$$Me^{n+} + S_2O_8^{2-} \rightarrow Me^{(n+1)+} + SO_4^{\bullet-} + SO_4^{2-} \tag{5}$$

$$Me^{n+}SO_4^{\bullet-} \rightarrow Me^{(n+1)+} + SO_4^{2-} \tag{6}$$

$$Dye + SO_4^{\bullet-} \rightarrow Oxidation\ products. \tag{7}$$

To identify the degradation mechanism, quenching studies were performed. It is well-known that alcohols with alpha-H, such as CH_3OH and CH_3CH_2OH readily react with hydroxyl and sulfate

Table 2. Kinetic constants of MO degradation at different temperatures on $Co_{2.4}Al_{3.1}Mn_{2.8}$ catalyst

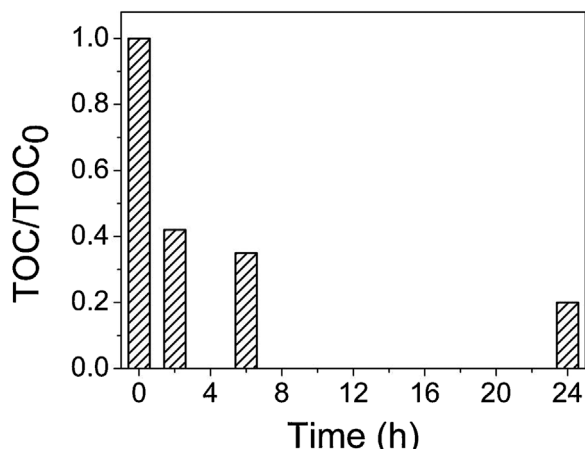| Sample	Temperature (°C)	k ($L\,s^{-1}\,mg^{-1}$)	R^2
$Co_{2.4}Al_{3.1}Mn_{2.8}$	30	2.40×10^{-4}	0.99
	40	2.88×10^{-4}	0.98
	50	3.71×10^{-4}	0.99

Figure 8. TOC removal of MO degradation by $Co_{7.9}Mn_0$ catalyst.

radicals. Thus, these alcohols are radical inhibitors because they are highly reactive toward active radical species [49, 50]. Peroxymonosulfate radicals, however, are relatively inert toward alcohols. The reaction of MO degradation by PS oxidation was carried out over $Co_{7.9}Mn_0$ catalyst in the presence of ethanol and *tert*-butyl alcohol. The same profiles as those presented in Fig. 6 (∇) were obtained, showing that $SO_4^{\bullet-}$ radicals would not be responsible for MO oxidation (data not shown).

Therefore, another oxidant species rather than sulfate radical generated from PS, would be responsible for MO oxidation. Several oxidant species based on PS are known, as HSO_4^- and peroxymonopersulfate anions, HSO_5^- [51]. The following reactions depict their formation:

$$S_2O_8^{2-} + H_2O \rightarrow HSO_5^- + HSO_4^- \qquad E^0 = 1.44\,V \qquad (8)$$

$$S_2O_8^{2-} + 2\,H^+ + 2\,e^- \rightarrow 2\,HSO_4^- \qquad E^0 = 2.12\,V. \qquad (9)$$

Taking into account that these species are formed under strong acidic conditions and that $SO_4^{\bullet-}$ and hydroxyl radicals were proved not to be involved in the reaction, it is likely that peroxymonopersulfates are responsible for MO oxidation. In line with this
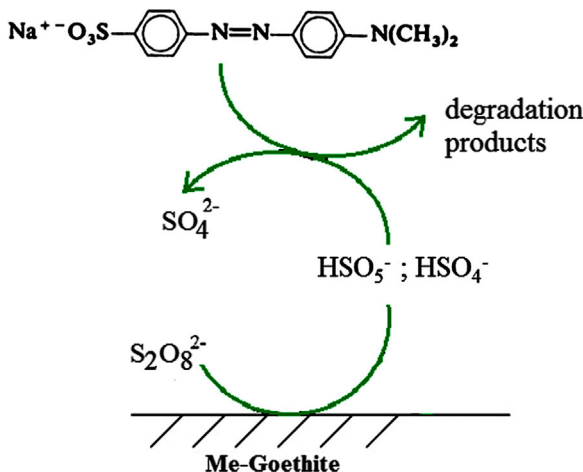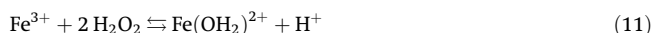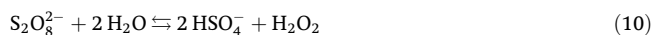

Figure 9. Proposed mechanism of MO degradation.

supposition, when the reaction was carried out under slight acidic conditions (pH 6) the degree of MO degradation was extremely low, due to the fact that peroxymonopersulfates are not generated under this condition (Supporting Information Fig. S3). For these reasons, it could be postulated that substituted goethites catalyze the formation of peroxymonopersulfates, under acidic conditions. These observations are in line with a similar mechanism proposed by Petri et al. [51] for Fe(III) systems. The authors state that the reduction of Fe(III) to Fe(II) probably takes place according to:

$$S_2O_8^{2-} + 2\,H_2O \leftrightharpoons 2\,HSO_4^- + H_2O_2 \qquad (10)$$

$$Fe^{3+} + 2\,H_2O_2 \leftrightharpoons Fe(OH_2)^{2+} + H^+ \qquad (11)$$

$$Fe(OH_2)^{2+} \rightarrow Fe^{2+} + HO_2^{\bullet} \qquad (12)$$

$$Fe^{3+} + HO_2^{\bullet} \rightarrow Fe^{2+} + O_2 + H^+. \qquad (13)$$

Accordingly, trivalent cations located inside the goethite structure could behave in a similar way.

The degradation pathway is summarized as follows in Fig. 9.

4 Concluding remarks

In the light of the results, it is possible to conclude that goethite oxides substituted with different metal heteroatoms (Co, Mn, and Al) are active toward MO degradation in acidic media. The highest conversion level was attained over the threefold-substituted goethite. Persulfate is activated over the heteroatom sites on the goethite surface. A radical based mechanism discarded in acidic media and peroxymonopersulfate may be the species involved in MO oxidation. The catalysts resulted quite stable under reaction conditions and the process followed a mechanism of oxidative degradation, favored by the presence of the transition metals Mn, Al, and Co, which activate PS. The TOC removal efficiency reached 80% when the reaction time was 24 h. The oxides could be easily recovered and reused. The application of these materials could result beneficial both from the economic and environmental point of view.

Acknowledgments

The authors have declared no conflict of interest.

References

[1] F. I. Hai, K. Yamamoto, K. Fukushi, Hybrid Treatment Systems for Dye Wastewater, Critical Reviews, *Environ. Sci. Technol.* **2007**, *37*, 315−377.

[2] Y. L. Song, J. T. Li, Degradation of C.I. Direct Black 168 From Aqueous Solution by Fly Ash/H_2O_2 Combining Ultrasound, *Ultrason. Sonochem.* **2009**, *16*, 440−444.

[3] L. Sun, Y. Yao, L. Wang, Y. Mao, Z. Huang, D. Yao, W. Lu, et al., Efficient Removal of Dyes Using Activated Carbon Fibers Coupled With 8-Hydroxyquinoline Ferric as a Reusable Fenton-Like Catalyst, *Chem. Eng. J.* **2014**, *240*, 413−419.

[4] D. Li, D. Chen, Y. Yao, J. Lin, F. Gong, L. Wang, L. Luo, et al., Strong Enhancement of Dye Removal Through Addition of Sulfite to Persulfate Activated by a Supported Ferric Citrate Catalyst, *Chem. Eng. J.* **2016**, *288*, 806–812.

[5] M. Neam, C. Zaharia, C. Catrinescu, A. Yediler, M. Macoveanu, A. Kettrup, Fe- Exchanged Y Zeolite as Catalyst for Wet Peroxide Oxidation of Reactive Azo Dye Procion Marine H-EXL, *Appl. Catal. B* **2004**, *48*, 287–294.

[6] Y. Zhan, X. Zhou, B. Fu, Y. Chen, Catalytic Wet Peroxide Oxidation of Azo Dye (Direct Blue 15) Using Solvothermally Synthesized Copper Hydroxide Nitrate as Catalyst, *J. Hazard. Mater.* **2011**, *187*, 348–354.

[7] L. Hua, H. Ma, L. Zhang, Degradation Process Analysis of the Azo Dyes by Catalytic Wet Air Oxidation with Catalyst CuO/γ-Al$_2$O$_3$, *Chemosphere* **2013**, *90*, 143–149.

[8] S. Athalathil, F. Stüber, C. Bengoa, J. Font, A. Fortuny, A. Fabregat, Characterization and Performance of Carbonaceous Materials Obtained From Exhausted Sludges for the Anaerobic Biodecolorization of the Azo Dye Acid Orange II, *J. Hazard. Mater.* **2014**, *267*, 21–30.

[9] B. Krishnakumar, T. Imae, J. Miras, J. Esquena, Synthesis and Azo Dye Photodegradation Activity of ZrS$_2$-ZnO Nano-Composites, *Sep. Purif. Technol.* **2014**, *132*, 281–288.

[10] M. Hou, F. Li, X. Liu, X. Wang, H. Wan, The Effect of Substituent Groups on the Reductive Degradation of Azo Dyes by Zerovalent Iron, *J. Hazard. Mater.* **2007**, *145*, 305–314.

[11] C. P. Huang, Y. F. Huang, H. P. Cheng, Y. H. Huang, Kinetic Study of an Immobilized Iron Oxide for Catalytic Degradation of Azo Dye Reactive Black B With Catalytic Decomposition of Hydrogen Peroxide, *Catal. Commun.* **2009**, *10*, 561–566.

[12] J. Bolobajev, E. Kattel, M. Viisimaa, A. Goi, M. Trapido, T. Tenno, N. Dulova, Reuse of Ferric Sludge as an Iron Source for the Fenton-Based Process in Wastewater Treatment, *Chem. Eng. J.* **2014**, *255*, 8–13.

[13] M. Stoyanova, I. Slavova, S. Christoskova, V. Ivanova, Catalytic Performance of Supported Nanosized Cobalt and Iron-Cobalt Mixed Oxides on MgO in Oxidative Degradation of Acid Orange 7 Azo Dye With Peroxymonosulfate, *Appl. Catal. A* **2014**, *476*, 121–132.

[14] T. Zhou, X. Wu, J. Mao, Y. Zhang, T. Lim, Rapid Degradation of Sulfonamides in a Novel Heterogeneous Sonophotochemical Magnetite-Catalyzed Fenton-Like (US/UV/Fe$_3$O$_4$/Oxalate) System, *Appl. Catal. B* **2014**, *160–161*, 325–334.

[15] F. Herrera, A. Lopez, G. Mascolo, P. Albers, J. Kiwi, Catalytic Combustion of Orange II on Hematite: Surface Species Responsible for the Dye Degradation, *Appl. Catal. B* **2001**, *29*, 147–162.

[16] I. R. Guimaraes, A. Giroto, L. C. A. Oliveira, M. C. Guerreiro, D. Q. Lima, J. D. Fabris, Synthesis and Thermal Treatment of Cu-Doped Goethite: Oxidation of Quinoline Through Heterogeneous Fenton Process, *Appl. Catal. B* **2009**, *91*, 581–586.

[17] Z. R. Lin, X. H. Ma, L. Zhao, Y. H. Dong, Kinetics and Products of PCB28 Degradation Through a Goethite-Catalyzed Fenton-Like Reaction, *Chemosphere* **2008**, *101*, 15–20.

[18] S. Rahim Pouran, A. A. Abdul Raman, W. M. A. W. Daud, Review on the Application of Modified Iron Oxides as Heterogeneous Catalysts in Fenton Reactions, *J. Cleaner Prod.* **2014**, *64*, 24–35.

[19] Y. Wang, Y. Gao, L. Chen, H. Zhang, Goethite as an Efficient Heterogeneous Fenton Catalyst for the Degradation of Methyl Orange, *Catal. Today* **2015**, *252*, 107–112.

[20] A. R. Laiju, T. Sivasankar, P. V. Nidheesh, Iron- Loaded Mangosteen as a Heterogeneous Fenton Catalyst for the Treatment of Landfill Leachate, *Environ. Sci. Pollut. Res. Int.* **2014**, *21*, 10900–10907.

[21] S. Xavier, R. Gandhimathi, P. V. Nidheesh, S. T. Ramesh, Comparison of Homogeneous and Heterogeneous Fenton Processes for the Removal of Reactive Dye Magenta MB From Aqueous Solution, *Desalin. Water Treat.* **2013**, *53*, 109–118.

[22] P. V. Nidheesh, Heterogeneous Fenton Catalysts for the Abatement of Organic Pollutants From Aqueous Solution: A Review, *RSC Adv.* **2015**, *5*, 40552–40577.

[23] P. V. Nidheesh, R. Gandhimathi, S. Velmathi, N. S. Sanjini, Magnetite as a Heterogeneous Electro Fenton Catalyst for the Removal of Rhodamine B From Aqueous Solution, *RSC Adv.* **2014**, *4*, 5698–5708.

[24] G. B. de la Plata, O. M. Alfano, A. E. Cassano, Decomposition of 2- Chlorophenol Employing Goethite as Fenton Catalyst. I. Proposal of a Feasible, Combined Reaction Scheme of Heterogeneous and Homogeneous Reactions, *Appl. Catal. B* **2010**, *95*, 1–13.

[25] A. M. Mesquita, I. R. Guimarães, G. M. M. de Castro, M. A. Gonçalves, T. C. Ramalho, M. C. Guerreiro, Boron as a Promoter in the Goethite (α-FeOOH) Phase: Organic Compound Degradation by Fenton Reaction, *Appl. Catal. B* **2016**, *192*, 286–295.

[26] H. Zhang, H. Fu, Y. Wang, L. Chen, Decolorization of Orange II by Heterogeneous Fenton Process Using Goethite as Catalyst, *Environ. Eng. Manage. J.* **2015**, *14*, 737–744.

[27] M. C. Pereira, L. C. A. Oliveira, E. Murad, Iron Oxide Catalysts: Fenton and Fenton-Like Reactions – A Review, *Clay Miner.* **2012**, *47*, 285–302.

[28] R. M. Cornell, U. Schwertmann, *The Iron Oxides: Structure, Properties, Reactions, Occurrences and Uses*, 2nd ed., Wiley-VCH, Weinheim, Germany **2003**.

[29] R. M. Cornell, Simultaneous Incorporation of Mn, Ni and Co in the Goethite (α-FeOOH) Structure, *Clay Miner.* **1991**, *26*, 427–430.

[30] A. Manceau, M. L. Schlegel, M. Musso, V. A. Sole, C. Gauthier, P. E. Petit, F. Trolard, Crystal Chemistry of Trace Elements in Natural and Synthetic Goethite, *Geochim. Cosmochim. Acta* **2000**, *64*, 3643–3661.

[31] M. Alvarez, E. E. Sileo, E. H. Rueda, Simultaneous Incorporation of Mn and Al in the Goethite Structure, *Geochim. Cosmochim. Acta* **2007**, *71*, 1009–1020.

[32] N. Kaur, M. Gräfe, B. Singh, B. J. Kennedy, Simultaneous Incorporation of Cr, Zn, Cd, and Pb in the Goethite Structure, *Clays Clay Miner.* **2009**, *57*, 234–250.

[33] N. Kaur, B. Singh, B. J. Kennedy, Copper Substitution Alone and in the Presence of Chromium, Zinc, Cadmium and Lead in Goethite (α-FeOOH), *Clay Miner.* **2009**, *44*, 293–310.

[34] M. Alvarez, A. E. Tufo, C. Zenobi, C. P. Ramos, E. E. Sileo, Chemical, Structural and Hyperfine Characterization of Goethites With Simultaneous Incorporation of Manganese, Cobalt and Aluminum Ions, *Chem. Geol.* **2015**, *414*, 16–27.

[35] J. Zhong, J. Li, Y. Lu, S. Huang, W. Hu, Oxidation of Methyl Orange Solution With Potassium Peroxydisulfate, *Iran. J. Chem. Chem. Eng.* **2012**, *31*, 21–24.

[36] B. H. Hameed, T. W. Lee, Degradation of Malachite Green in Aqueous Solution by Fenton Process, *J. Hazard. Mater.* **2009**, *164*, 468–472.

[37] H. Van Olphen, *An Introduction to Clay Colloid Chemistry*, Wiley, New York **1977**.

[38] M. Kosmulski, Compilation of PZC and IEP of Sparingly Soluble Metal Oxides and Hydroxides From Literature, *Adv. Colloid Interface Sci.* **2009**, *152*, 14–25.

[39] A. J. Aquino, D. Tunega, G. Haberhauer, M. H. Gerzabek, H. Lischka, Quantum Chemical Adsorption Studies on the (110) Surface of the Mineral Goethite, *J. Phys. Chem. C* **2007**, *111*, 877–885.

[40] M. Alvarez, E. E. Sileo, E. H. Rueda, Structure and Reactivity of Synthetic Co-substituted Goethites, *Am. Mineral.* **2008**, *93*, 584–590.

[41] L. Qin, Y. H. Li, P. J. Ma, G. H. Cui, Exploring the Effect of Chain Length of Bridging Ligands in Cobalt(II) Coordination Polymers Based on Flexible Bis(5,6-dimethylbenzimidazole) Ligands: Synthesis, Crystal Structures, Fluorescence and Catalytic Properties, *J. Mol. Struct.* **2013**, *1051*, 215–220.

[42] H. Liu, T. Chen, R. L. Frost, An Overview of the Role of Goethite Surfaces in the Environment, *Chemosphere* **2014**, *103*, 1–11.

[43] J. Fan, Y. Guo, J. Wang, M. Fan, Rapid Decolorization of Azo Dye Methyl Orange in Aqueous Solution by Nanoscale Zerovalent Iron Particles, *J. Hazard. Mater.* **2009**, *166*, 904–910.

[44] G. Blanchard, M. Maunaye, G. Martin, Removal of Heavy Metals From Waters by Means of Natural Zeolites, *Water Res.* **1984**, *18*, 1501–1507.

[45] H. Wu, X. Dou, D. Deng, Y. Guan, L. Zhang, G. He, Decolourization of the Azo Dye Orange G in Aqueous Solution via a Heterogeneous Fenton-Like Reaction Catalysed by Goethite, *Environ. Technol.* **2012**, *33*, 1545–1552.

[46] Y. H. Shih, C. P. Tso, L. Y. Tung, Rapid Degradation of Methyl Orange with Nanoscale Zerovalent Iron Particles, *J. Environ. Eng. Manage.* **2010**, *20*, 137–143.

[47] H. Kusic, I. Peternel, S. Ukic, N. Koprivanac, T. Bolanca, S. Papic, A. L. Bozic, Modeling of Iron Activated Persulfate Oxidation Treating Reactive Azo Dye in Water Matrix, *Chem. Eng. J.* **2011**, *172*, 109–121.

[48] C. S. Liu, K. Shih, C. X. Sun, F. Wang, Oxidative Degradation of Propachlor by Ferrous and Copper Ion Activated Persulfate, *Sci. Total Environ.* **2012**, *416*, 507–512.

[49] G. P. Anipsitaki, D. D. Dionysiou, Radical Generation by the Interaction of Transition Metals With Common Oxidants, *Environ. Sci. Technol.* **2004**, *38*, 3705–3712.

[50] G. P. Anipsitakis, D. D. Dionysiou, Degradation of Organic Contaminants in Water With Sulfate Radicals Generated by the Conjunction of Peroxymonosulfate With Cobalt, *Environ. Sci. Technol.* **2003**, *37*, 4790–4790.

[51] B. G. Petri, R. J. Watts, A. Tsitonaki, M. Crimi, N. R. Thomson, A. L. Teel, *In Situ Chemical Oxidation for Groundwater Remediation* (Eds.: R. L. Siegrist, M. Crimi, T. J. Simpkin, Springer, New York **2011**, p. 147.